Cancer Science
Japanese Cancer Association JCA
Open Access

Radiolabeled liposome imaging determines an indication for liposomal anticancer agent in ovarian cancer mouse xenograft models

Ken Ito,[1,2,5] Shusei Hamamichi,[2,5] Makoto Asano,[3] Yusaku Hori,[2,3] Junji Matsui,[3] Masao Iwata,[3] Yasuhiro Funahashi,[4] Izumi O. Umeda[2] and Hirofumi Fujii[2]

[1]Halichondrin Research Laboratory, Eisai Co., Ltd., Tsukuba, Japan; [2]Division of Functional Imaging, National Cancer Center, Kashiwa, Japan; [3]Oncology Product Creation Unit, Eisai Co., Ltd., Tsukuba, Japan; [4]Biomarkers and Personalized Medicine Core Function Unit, Eisai Inc., Andover, Massachusetts, USA

Key words

Doxil, ovarian cancer, radiolabeled liposomes, single-photon emission computed tomography/computed tomography imaging, theranostics

Correspondence

Hirofumi Fujii, Division of Functional Imaging, Exploratory Oncology Research and Clinical Trial Center, National Cancer Center, 6-5-1 Kashiwanoha, Kashiwa, Chiba 277-8577, Japan.
Tel: +81-4-7134-6832; Fax: +81-4-7134-6832;
E-mail: hifujii@east.ncc.go.jp

Funding Information

Japan Society for the Promotion of Science; Eisai, Co., Ltd. under contract with the National Cancer Center, Japan.

[5]These authors contributed equally to this work.

Received July 24, 2015; Revised October 15, 2015; Accepted October 23, 2015

Cancer Sci **107** (2016) 60–67

doi: 10.1111/cas.12841

Liposomal anticancer agents can effectively deliver drugs to tumor lesions, but their therapeutic effects are enhanced in only limited number of patients. Appropriate biomarkers to identify responder patients to these liposomal agents will improve their treatment efficacies. We carried out pharmacological and histopathological analyses of mouse xenograft models bearing human ovarian cancers (Caov-3, SK-OV-3, KURAMOCHI, and TOV-112D) to correlate the therapeutic effects of doxorubicin-encapsulated liposome (Doxil®) and histological characteristics linked to the enhanced permeability and retention effect. We next generated ^{111}In-encapsulated liposomes to examine their capacities to determine indications for Doxil® treatment by single-photon emission computed tomography (SPECT)/CT imaging. Antitumor activities of Doxil® were drastically enhanced in Caov-3, moderately in SK-OV-3, and minimally in KURAMOCHI and TOV-112D when compared to doxorubicin. Microvessel density and vascular perfusion were high in Caov-3 and SK-OV-3, indicating a close relation with the enhanced antitumor effects. Next, ^{111}In-encapsulated liposomes were given i.v. to the animals. Their tumor accumulation and area under the curve values over 72 h were high in Caov-3, relatively high in SK-OV-3, and low in two other tumors. Importantly, as both Doxil® effects and liposomal accumulation varied in the SK-OV-3 group, we individually obtained SPECT/CT images of SK-OV-3-bearing mouse (n = 11) before Doxil® treatment. Clear correlation between liposomal tumor accumulation and effects of Doxil® was confirmed (R^2 = 0.73). Taken together, our experiments definitely verified that enhanced therapeutic effects through liposomal formulations of anticancer agents depend on tumor accumulation of liposomes. Tumor accumulation of the radiolabeled liposomes evaluated by SPECT/CT imaging is applicable to appropriately determine indications for liposomal antitumor agents.

Currently, several liposomal anticancer agents are approved by the FDA to treat the following cancers: doxorubicin-encapsulated liposomes (Doxil®) for ovarian cancer, breast cancer, and Kaposi's sarcoma; daunorubicin-encapsulated liposomes (DaunoXome®) for Kaposi's sarcoma; vincristine-encapsulated liposomes (Marqibo®) for acute lymphoblastic leukemia; and cytarabine-encapsulated liposomes (DepoCyt®) for lymphomatous meningitis.[1,2] Additional liposomal agents are under investigation towards their clinical application. It is expected that advantages of liposomal anticancer agents include tumor-selective targeting of macromolecules based on the concept of the enhanced permeability and retention (EPR) effect, which consequently leads to higher accumulation of free drugs in the tumor, and reduction of side-effects that are related to their free drugs.[3–6] For example, liposomal formulations of doxorubicin and daunorubicin, as well as vincristine and cytarabine, reduced side-effects such as cardiotoxicity and hematological toxicity, respectively, leading to improved overall compliance and quality of life for cancer patients.[7–10] Due to progressive development of technology related to improvement of drug delivery systems, as well as the expansion of the aging population worldwide with cancer, the number of liposomal as well as lipid-based anticancer agents is expected to increase.

Despite the expected advantages, liposomal agents provide clinical benefits for only a limited number of cancer patients. Indeed, the overall response rate (complete response or partial response [PR]) was 19.7% for Doxil® in recurrent epithelial ovarian carcinoma, 25% for DaunoXome® in AIDS-related Kaposi's sarcoma, 25% for Marqibo® in refractory aggressive non-Hodgkin's lymphoma, and 26% for DepoCyt® in a clinical trial with solid tumor patients.[11–13] These records indicate that there is a necessity to evaluate tumor characteristics that are favorable for liposomal anticancer agents and, based on these findings, to develop biomarkers that are capable of predicting efficacies of liposomal agents.

In recent years, importance of diagnostic imaging has been emphasized for treatment planning of many diseases, especially cancer. Within nanomedicine, there are particularly interesting possibilities to generate nanocarriers that can be engineered to transport diagnostic and therapeutic agents, a concept termed theranostics.[14,15] Several theranostic procedures have already been used in routine clinical practice. For example, when octreotide (a synthetic analog of somatostatin that binds to somatostatin receptors) is labeled with positron-emitting ^{68}Ga, expression of somatostatin receptors on tumors can be visualized, and positive scintigraphic findings allow us to proceed to radionuclide therapy to treat gastroenteropancreatic neuroendocrine tumors with radiolabeling of octreotide with Auger electron- and β-emitting ^{90}Y or ^{177}Lu.[16] Applying this concept to the liposomal agents, we listed the current set of FDA-approved liposomal anticancer agents, specifically focusing on their lipid compositions and sizes, and examined if we could generate diagnostic versions of the therapeutic liposomes by altering the interior contents from encapsulation of anticancer agents to radionuclides. Although a few radiolabeled liposomes have already been proposed as nanocarriers for theranostic applications,[17–19] their usefulness has not been clearly determined and no effective biomarkers for these liposomal agents have been established yet.

As a strategy to develop the biomarkers with capacities to predict the effectiveness of liposomal anticancer agents, we initially compared the pharmacological effects of Doxil® and doxorubicin among mouse xenograft models bearing four different human ovarian cancers (Caov-3, SK-OV-3, KURAMOCHI, and TOV-112D), and carried out histopathological analyses to correlate the therapeutic effects of Doxil® and histological characteristics linked to EPR. We clearly showed a close correlation between them. We next generated ^{111}In-encapsulated liposomes with lipid composition and size identical to Doxil®, and applied single-photon emission computed tomography (SPECT)/CT imaging of the aforementioned mouse xenograft models. Differing accumulation levels of the radiolabeled liposomes offered a unique opportunity to investigate the feasibility of the radiolabeled liposomes to individually diagnose and predict the efficacy of Doxil® treatment. Hence, we examined each xenografted mouse to determine tumor accumulation of the radiolabeled liposomes by SPECT/CT imaging and, remarkably, we confirmed a clear correlation between the accumulation and the effects of liposomal formulation. Our integrated preclinical findings showed the merit of the radiolabeled liposomes, designed for SPECT/CT imaging, as imaging biomarkers to decide the indications for Doxil® treatment.

Materials and Methods

Cell lines and culture conditions. Human ovarian cancer cell lines, Caov-3, SK-OV-3, and TOV-112D were obtained from ATCC (Manassas, VA, USA), and KURAMOCHI from the Health Science Research Resources Bank (Osaka, Japan). Culture conditions are described in Data S1.

Human ovarian cancer xenograft models. All animal studies were approved by the Eisai Institutional Animal Care and Use Committee (Tsukuba, Japan), as well as the Institutional Animal Experimental Committee at the National Cancer Center (Kashiwa, Japan). Caov-3, SK-OV-3, KURAMOCHI, and TOV-112D cells were suspended with 50% BD Matrigel (Becton Dickinson, Tokyo, Japan) and 5–1000 × 10^6 cells were inoculated s.c. in 7-week-old female nude mice (CAnN.Cg-Foxn1nu/CrlCrlj) (Charles River Japan, Atsugi, Japan).

Antitumor activities of Doxil® and doxorubicin in human ovarian cancer mouse xenograft models. Approximately 1–3 weeks after transplantation, 10 mg/kg (the maximum tolerated dose) of doxorubicin (Adriacin®; Kyowa Hakko Kirin Co., Ltd., Tokyo, Japan) or Doxil® were given i.v. to four different human ovarian cancer xenograft models. The tumor volume (TV) and the body weight were measured twice a week. Tumor volume was calculated according to the formula: TV (mm^3) = length (mm) × width (mm) × width (mm) × 1/2. The relative TV (RTV) was calculated according to the formula: RTV = TV on Day n/TV on Day 1.

Accumulation levels of Doxil® and histopathological analysis of xenograft models. Tumor vascular perfusion was evaluated by i.v. injection of Doxil® as well as Hoechst 33342 dye (Invitrogen, Eugene, OR, USA),[20] and phenotypes of tumor vessels were evaluated as microvessel density (MVD) by staining with anti-CD31 antibodies. Detailed information is available in Data S1.

Preparation of ^{111}In-encapsulated liposomes. We developed ^{111}In-diethylene-triamine-pentaacetic acid-encapsulated liposomes (^{111}In-encapsulated liposomes) with the same lipid 689e of Doxil®. These liposomes were prepared by the lipid film hydration extrusion method, followed by the remote loading method.[21,22] Preparation of the radiolabeled liposomes, and subsequent *in vitro* stability assay are further explained in Data S1.

***Ex vivo* biodistribution of ^{111}In-encapsulated liposomes.** ^{111}In-encapsulated liposomes (400–600 kBq/2 μmol HSPC/0.2 mL saline) were injected i.v. into tumor-bearing nude mice. At 1, 24, 48, and 72 h after injection, we obtained blood, tumors, and other major organs, and measured radioactivities (count per minute [CPM]) by using an automatic γ-counter (Wizard^2 2480; PerkinElmer, Hopkinton, MA, USA). ^{111}In accumulation was calculated as % of administered dose/gram of organ (% AD/g) by using the formula:

$$\%\ \text{administered dose/gram of organ}\ (\%\text{AD/g}) = \frac{\text{CPM (organ)} \times 100}{\text{organ weight (g)} \times \text{CPM (administered dose)}}$$

Imaging. As a way to non-invasively monitor liposomal accumulation in the tumor, we acquired serial SPECT/CT images of the same animal at 1, 24, 48, and 72 h after injection of ^{111}In-encapsulated liposomes. The detailed information on SPECT/CT imaging is provided in Data S1.

Statistical analysis. Data are expressed as the mean ± SD. The Tukey multiple comparison test was used to evaluate the statistical significance among four ovarian cancer xenograft models. *P*-values lower than 0.05 were considered statistically significant.

Results

Antitumor activities of Doxil® and doxorubicin in human ovarian cancer mouse xenograft models. After establishment of Caov-3, SK-OV-3, KURAMOCHI, and TOV-112D tumors (starting tumor volume, 150–200 mm^3), Doxil® (10 mg/kg), a free form of Doxil®, and doxorubicin (10 mg/kg) were given i.v. to four different human ovarian cancer xenograft models. The time of administration was considered as day 1. We initially compared antitumor activities of Doxil® and doxorubicin among the tumor-bearing mice.

Antitumor effects of doxorubicin were different among four xenograft models, and the enhancement of pharmacological effects through liposomal formulation also varied among four kinds of tumor xenografts (Table S1). The enhancement of antitumor activity was drastic in Caov-3, moderate in SK-OV-3, and minimal in KURAMOCHI and TOV-112D (Fig. 1). There was no clear association between the effectiveness of Doxil® and doxorubicin *in vivo* (Table S1). These results suggested that characteristics of the tumors *in vivo*, presumably those related to the EPR effect, might influence effectiveness of the liposomal anticancer agent.

Accumulation levels of Doxil® in Caov-3 and SK-OV-3 xenograft models. As doxorubicin, which is encapsulated in Doxil®, is autofluorescent, we further investigated the correlation between the pharmacological effects of Doxil® and its tumor accumulation, although as expected, our method could not distinguish intact Doxil® from its released doxorubicin. At 24 h after injection, we resected tumor samples, and quantified fluorescent intensities. The accumulation level of Doxil® in Caov-3, evaluated by the autofluorescent intensity was significantly higher than other three tumor types (Fig. 2). Furthermore, although not as significant as Caov-3, accumulation of Doxil® in SK-OV-3 was also high when compared to KURAMOCHI and TOV-112D. As both Caov-3 and SK-OV-3 were sensitive to Doxil® compared with doxorubicin, these results suggested that delivery and retention are critical factors that are necessary for enhanced antitumor activities.

Histopathological analyses of the ovarian cancer xenografted tumors. We next carried out a perfusion assay using Hoechst 33342 staining, a fluorescent marker for tumor perfusion, combined with an endothelial marker, anti-CD31 immunostaining.[20] We hypothesized that, as the effectiveness of Doxil® was related to its delivery and retention, analyses of histopathological characteristics associated with vascular perfusion and MVD might provide mechanistic insights to distinguish tumor types with or without responses to Doxil® treatment. The tumor blood perfusion was calculated as Hoechst-positive area in cryosections of frozen tumor specimens. As expected, the Hoechst-positive region indicating blood perfusion was significantly higher in Caov-3 and SK-OV-3 xenografted tumors than in the other two types (Fig. 2b, d). We next characterized phenotypes of tumor vessels by staining with anti-CD31 antibodies, and we observed significantly high MVDs in Caov-3 and SK-OV-3 (Fig. 2b,e). These results indicated that Caov-3 and SK-OV-3 xenografted tumors possessed highly perfuse characteristics, which led to elevated accumulation levels and enhanced antitumor activities of Doxil®.

Biodistribution of ^{111}In-encapsulated liposomes in human ovarian cancer mouse xenograft models. We next explored tumor accumulation and biodistribution patterns of the radiolabeled liposomes at 1, 24, 48, and 72 h after injection in four ovarian cancer xenograft models. Accumulation levels of these radiolabeled liposomes in the tumors and the other organs were expressed as %AD/g. Before the injection of radiolabeled liposomes, the stability of these liposomes was confirmed (Table S2).

Figure 3(a) shows a time-course analysis of the ^{111}In-encapsulated liposomes that accumulated in the tumors. The accumulation in Caov-3 tumors increased after the injection and reached the peak of 5.8 ± 1.9 %AD/g at 24 h. The accumulation continued until 48 h after the injection, and afterwards, it gradually decreased. The accumulation in SK-OV-3 tumors increased throughout the time points and reached 4.3 ± 2.4 % AD/g at 72 h after injection. Although the accumulation levels in KURAMOCHI and TOV-112D tumors increased at 24–48 h after injection, the peaks were as low as 2%AD/g. Based on these biodistribution patterns from 1 to 72 h, area under the curve (AUC) values were high in Caov-3 (338.0 arbitrary unit [AU]), followed by SK-OV-3 (254.7 AU) and the other two tumor types (Table 1). Collectively, these results correlated with antitumor activities of Doxil® wherein Doxil® was more effective in Caov-3 and SK-OV-3 than KURAMOCHI and TOV-112D.

Accumulation levels of the ^{111}In-encapsulated liposomes in each tumor at 72 h after the injection are summarized in Figure 3(b). While the averages of Caov-3 and SK-OV-3 were high, intertumoral variances were observed, especially SK-OV-3. Even in the same tumor xenograft models, the accumulation of ^{111}In-encapsulated liposomes varied. We did not recognize different accumulation patterns in major normal organs among four xenograft models (Table S3).

Imaging. Ovarian cancer xenografts from each tumor-bearing mouse (total, n = 3–5) were repeatedly imaged by a SPECT/CT scanner after the injection of ^{111}In-encapsulated liposomes. Representative SPECT/CT images of each tumor xenograft obtained at 1, 24, 48, and 72 h after the injection are shown in Figure 4(a). As each tumor was implanted in the infra-axillary region and injected liposomes were likely to accumulate in the reticuloendothelial system, strong radioactivity in the liver was depicted in each image. Thorough observation of superimposed CT images enabled the radiologist to

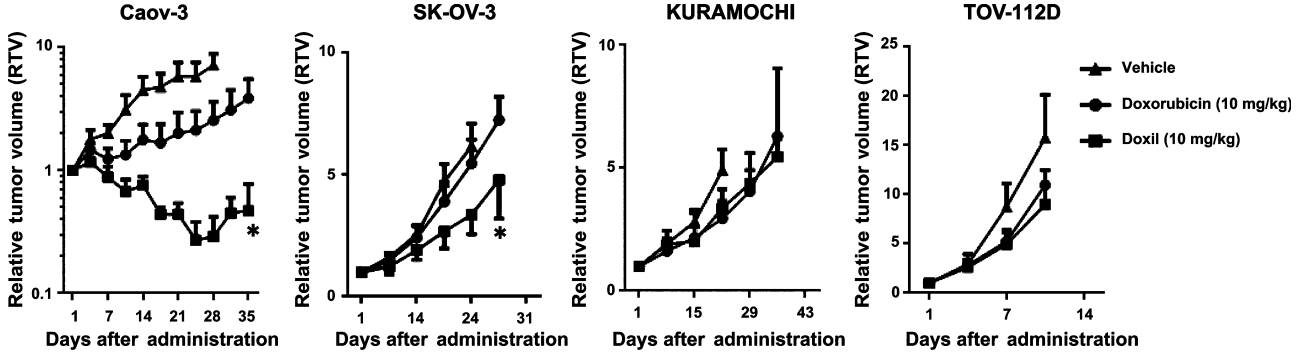

Fig. 1. Antitumor activities of doxorubicin-encapsulated liposome (Doxil®) and doxorubicin in human ovarian cancer xenograft models. The panels show *in vivo* efficacies of Doxil® and doxorubicin (n = 6, each group). The drugs were given i.v. at day 1. Comparison between antitumor activities of Doxil® and doxorubicin among four tumor-bearing mice revealed the effectiveness of Doxil® in Caov-3 and SK-OV-3 tumor xenografts, as well as that of doxorubicin in only Caov-3. Bars indicate SD. *P < 0.05 versus Doxil® (Student's t-test) on the same day.

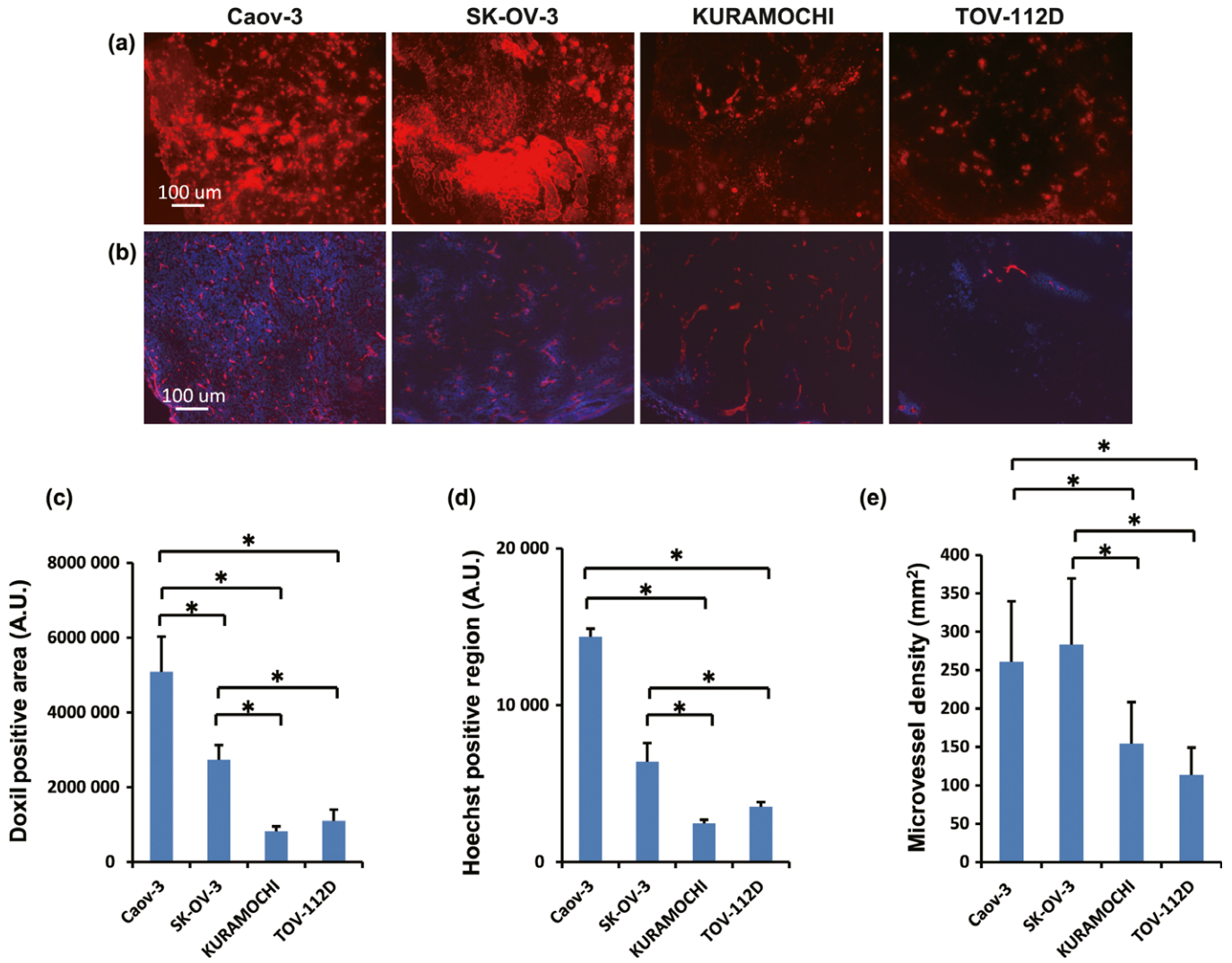

Fig. 2. Immunohistological analysis of tumor vasculature and microenvironment in human ovarian cancer mouse xenograft models. (a) Representative images of doxorubicin-encapsulated liposome (Doxil®) distribution in tumors (n = 5). (b) Representative images of Hoechst 33342 dye perfusion assay (blue) with CD31 staining (red) (n = 5). Hoechst-positive and CD31 stained regions were clearly depicted in Caov-3 and SK-OV-3 xenografted tumors, but not in KURAMOCHI or TOV-112D tumors. (c) Quantitative analyses of Doxil®-positive areas among these four tumor types. (d, e) Quantitative analyses of Hoechst 33342 dye perfusion (d), and microvessel density (MVD) (e). Data represent mean ± SD. *P < 0.05; each group consisted of five mice per group. AU, arbitrary unit.

properly put regions of interest (ROIs) on the tumor and measure the counts.

All Caov-3 tumors (n = 3) showed high accumulation of ^{111}In-encapsulated liposomes whereas SK-OV-3 tumors showed variable activity for each tumor. The representative images of both high and low activities are illustrated in Figure 4(a). No obvious activities were observed in KURAMOCHI or TOV-112D xenograft models. Representative serial SPECT/CT images of each tumor xenograft at 72 h after the injection are shown in Figure S1.

The time–activity curve of each xenograft model is shown in Figure 4(b). Consistent with the aforementioned biodistribution patterns of the radiolabeled liposomes in the tumors, the counts of Caov-3 tumors gradually increased after the injection and reached the peak at 48 h. Afterwards, the counts in the tumors decreased. The average counts of SK-OV-3 increased for up to 72 h after the injection, and the other two kinds of tumors showed low counts throughout the time period. Collectively, the radioactivities detected in the tumors as shown in Figure 4(b) were well correlated with signal intensities from the SPECT/CT images in Figure 4(a).

Correlation between accumulation of ^{111}In-encapsulated liposomes in the tumors and antitumor activity of Doxil® in xenograft models. Tumor accumulation of the ^{111}In-encapsulated liposomes varied among different tumor types. Furthermore, even when the same cancer cells were xenografted, accumulation levels of the radiolabeled liposomes were widely distributed. Specifically, SK-OV-3 tumor xenografts showed a great variety of both therapeutic efficacy of Doxil® and tumor accumulation of ^{111}In-encapsulated liposomes. This unique observation led us to evaluate their application to predict the therapeutic effects of Doxil® by SPECT/CT tumor images before the initiation of the treatment.

At 72 h after injection of the radiolabeled liposomes, we individually obtained SPECT/CT images of each SK-OV-3 bearing mouse (total, n = 11). To clearly visualize the tumor, this time point was selected because previous results showed that a large quantity of the radiolabeled liposomes

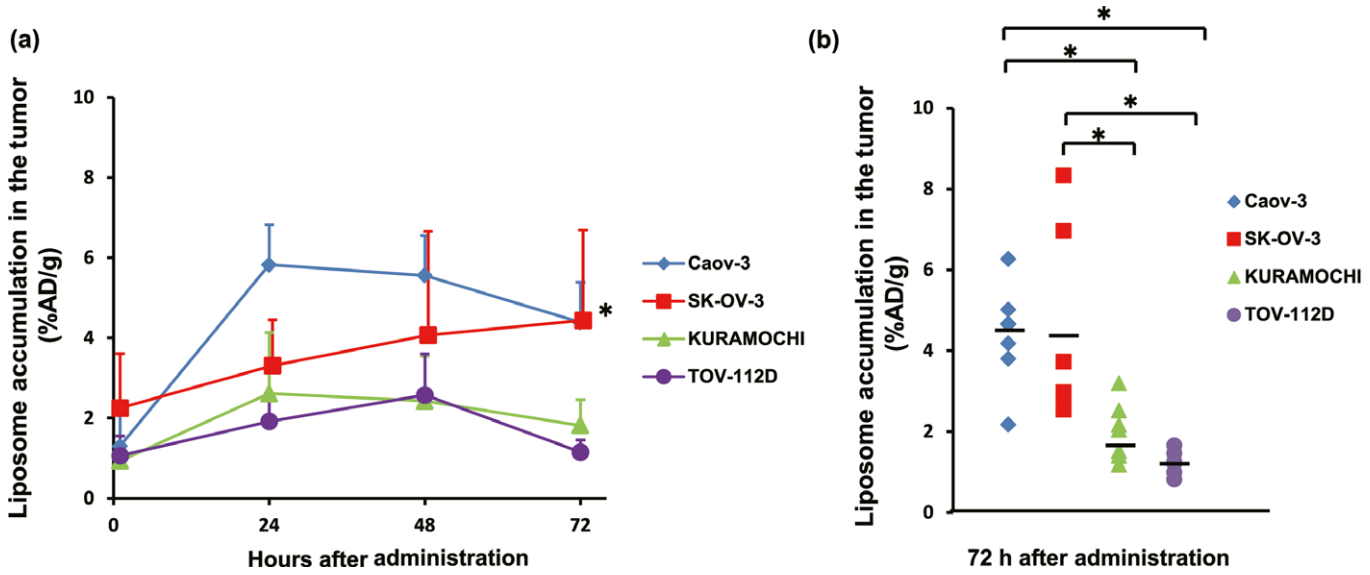

Fig. 3. *Ex vivo* accumulation of ^{111}In-encapsulated liposomes at several time points among four human ovarian cancer xenografted tumors. (a) *Ex vivo* analysis at each time point revealed significantly higher accumulation levels in Caov-3 and SK-OV-3 tumors than those in KURAMOCHI and TOV-112D tumors at 72 h after injection. Six to 11 mice were used for analysis in each group at each time point. (b) Accumulation of ^{111}In-encapsulated liposomes in an individual mouse at 72 h after injection. Most notably, among all four tumor types analyzed, only SK-OV-3 displayed a wide range of variation. *$P < 0.05$. %AD/g, % of administered dose/gram of organ.

Table 1. Area under the curve (AUC) values of ^{111}In-encapsulated liposomes in ovarian cancer xenografted tumors

	AUC (AU) from *ex vivo* distribution assay	AUC (AU) from SPECT/CT imaging
Caov-3	338.0	391.6
SK-OV-3	254.7	251.8
KURAMOCHI	152.3	91.7
TOV-112D	132.9	96.7

AUC values were calculated by using GraphPad Prism 6 Software. AU, arbitrary unit; CT, computed tomography; SPECT, single-photon emission computed tomography.

accumulated in the tumor while less remained in the blood, leading to better tumor-to-blood ratios of all tumor types examined. As we expected, the accumulation in SK-OV-3 varied at this time point (Fig. 5a). We then i.v. administered Doxil® to each mouse at the concentration of 10 mg/kg. Importantly, there was a clear correlation between accumulation levels of the radiolabeled liposomes and antitumor activities of Doxil® at day 12 with correlation factor of $R^2 = 0.73$ (Fig. 5b,c). These results indicated that the radiolabeled liposomes possess the potential to accurately predict the efficacies of Doxil®, suggesting an application towards personalized medicine.

Histopathological analyses of SK-OV-3 tumors. As accumulation of the liposomes varied in the SK-OV-3 xenografted tumors, we investigated their histopathological features to correlate perfusion levels, which is one of the most important factors to determine the accumulation of liposomes. Initially, we examined H&E and immunohistochemically stained SK-OV-3 tumors (Fig. S2a). Low perfusion tumor was stroma-rich and showed high collagen I intensity and low MVD, whereas high perfusion tumor had a small amount of stroma and showed low collagen I intensity and high MVD. Next, we examined perfusion levels of Hoechst 33342 in the multiple SK-OV-3 xenografted tumors ($n = 10$; Fig. S2b), and carried out correlation analyses between tumor perfusion and tumor weight (Fig. S2c), MVD (CD31) (Fig. S2d), hypoxic region (carbonic anhydrase 9) (Fig. S2e), and average collagen I intensity (Fig. S2f). Only MVD and average collagen I intensity correlated well with tumor perfusion. Taken together, comprehensive tumor tissue analyses suggested that increase of MVD and decrease of collagen I intensity are important histological factors for increased tumor perfusion and, consequently, accumulation of the liposomes in the SK-OV-3 xenograft model.

Discussion

In light of enhanced drug delivery to tumors, although liposomes encapsulating anticancer agents are potent, they are not effective to all malignant tumors. Thus, development of biomarkers to identify responder patients to liposomal agents is crucial. In this study, we initially examined the antitumor activities of liposomal anticancer agent, Doxil®, by comparing it to its free drug, doxorubicin, among xenograft models bearing four human ovarian cancers (Caov-3, SK-OV-3, KURAMOCHI, and TOV-112D). Differing responses of these four tumors to the anticancer agent were observed, that is, superior enhanced efficacies of Doxil® in Caov-3, relatively superior enhanced efficacies in SK-OV-3, and slight to no efficacies against KURAMOCHI and TOV-112D. In other animal models as well as ours, the liposomal anticancer agent is not expected to be efficacious against all cancer types. Observation of the autofluorescent doxorubicin in the tumor suggested that the tumor accumulation of Doxil® was higher in Caov-3 and SK-OV-3 than in others. The MVD and vascular perfusion were also high in Caov-3 and SK-OV-3. These results strongly indicated that enhanced antitumor activities of Doxil® depended on its tumor accumulation, which was closely associated with MVD and vascular perfusion.

These results strongly encouraged us to develop a strategy that would enable us to evaluate the tumor accumulation of

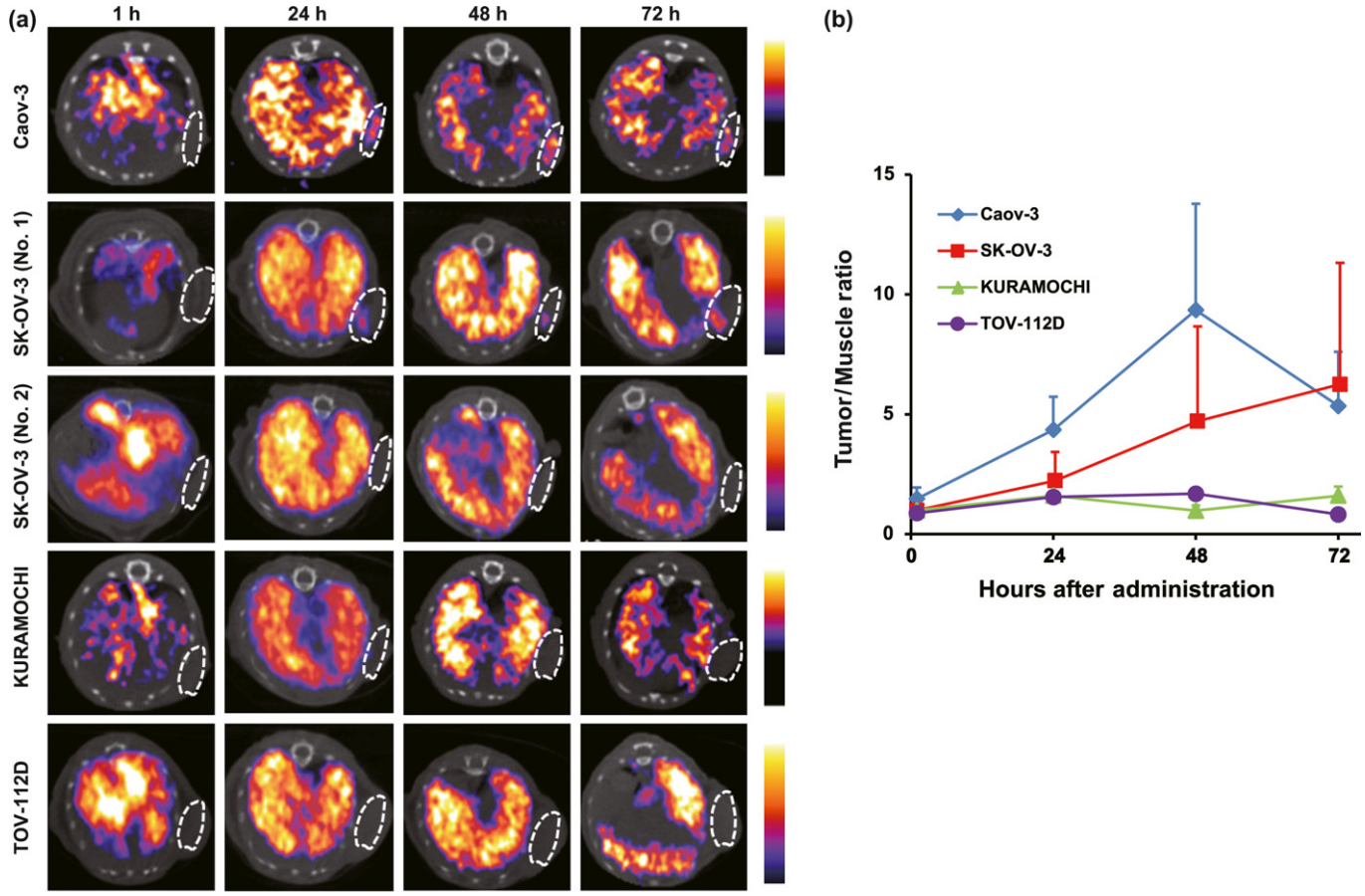

Fig. 4. Single-photon emission computed tomography (SPECT)/CT imaging of ^{111}In-encapsulated liposomes in human ovarian cancer mouse xenograft models. (a) Representative axial SPECT/CT images of mouse xenograft models (n = 3–5). White circle indicates tumor region based on superimposed CT image. High accumulation levels were observed in Caov-3, followed by SK-OV-3, tumors between 24 and 72 h. We observed interindividual variation in SK-OV-3 xenograft mice from 48 h with clear depiction of tumor (No. 1) or none (No. 2). (b) Tumor/background ratio from SPECT image data analysis.

liposomes *in vivo*. We generated ^{111}In-encapsulated liposomes with lipid composition and size identical to Doxil®. As both our radiolabeled liposomes and Doxil® were matching as liposomal nanocarriers, biodistribution patterns of these diagnostic and therapeutic liposomes were presumably indistinguishable. The accumulation levels of ^{111}In-encapsulated liposomes in tumors could be measured by counting γ-rays emitted from radionuclides.[23–26] Through optimization of procedures associated with encapsulation of radionuclides into the liposomes, their accumulation levels in tumors could be clearly imaged *in vivo* by SPECT/CT tests.

We initially measured the counts of ^{111}In-encapsulated liposomes that accumulated in the *ex vivo* tumors, and we thereafter carried out *in vivo* SPECT/CT imaging studies. The results of both studies were similar: their tumor accumulation levels and AUC values over 72 h were high in Caov-3, relatively high in SK-OV-3, and low in the other two tumor types. These measurements were consistent with those of the aforementioned retention and the enhanced therapeutic effects of Doxil® in four tumors. Importantly, as both Doxil® effects and liposomal accumulation varied in the SK-OV-3 group, we individually obtained SPECT/CT images of SK-OV-3-bearing mouse (n = 11) before Doxil® treatment. A clear correlation between the liposomal tumor accumulation and the effects of Doxil® was confirmed (R^2 = 0.73). Additionally, to further characterize SK-OV-3 xenografted tumors histologically, we carried out multiple histopathological analyses, and showed that a variety of MVD and collagen I intensity levels critically induced the diversity of tumor perfusion and accumulation of the liposomes in the SK-OV-3 xenograft models. These results suggested that accumulation levels of the radiolabeled liposomes could be applied as a biomarker to determine the indications for Doxil® treatment.

Antitumor activities of the liposomes originate from the encapsulated anticancer agents, but liposomal formulation is expected to not only reduce their side-effects, but also enhance their antitumor activities. Therefore, it is essential to evaluate the enhanced liposomal effect, likely dependent on the characteristics of the tumor microenvironment (e.g., MVD and vascular perfusion) leading to enhanced EPR effect and subsequent tumor accumulation in each patient.[27] Among cancer patients, the characteristics of the tumor microenvironment are different, which conceivably may explain the limited effectiveness of liposomal anticancer agents. Our radiolabeled liposomes are designed to evaluate the enhancement. Tumor accumulation of the radiolabeled liposomes evaluated by SPECT/CT imaging is ubiquitously applicable to determine indications for liposomal antitumor agents.[28,29] In addition, this method will also be effective for monitoring the course of treatment because the tumor microenvironment is likely to

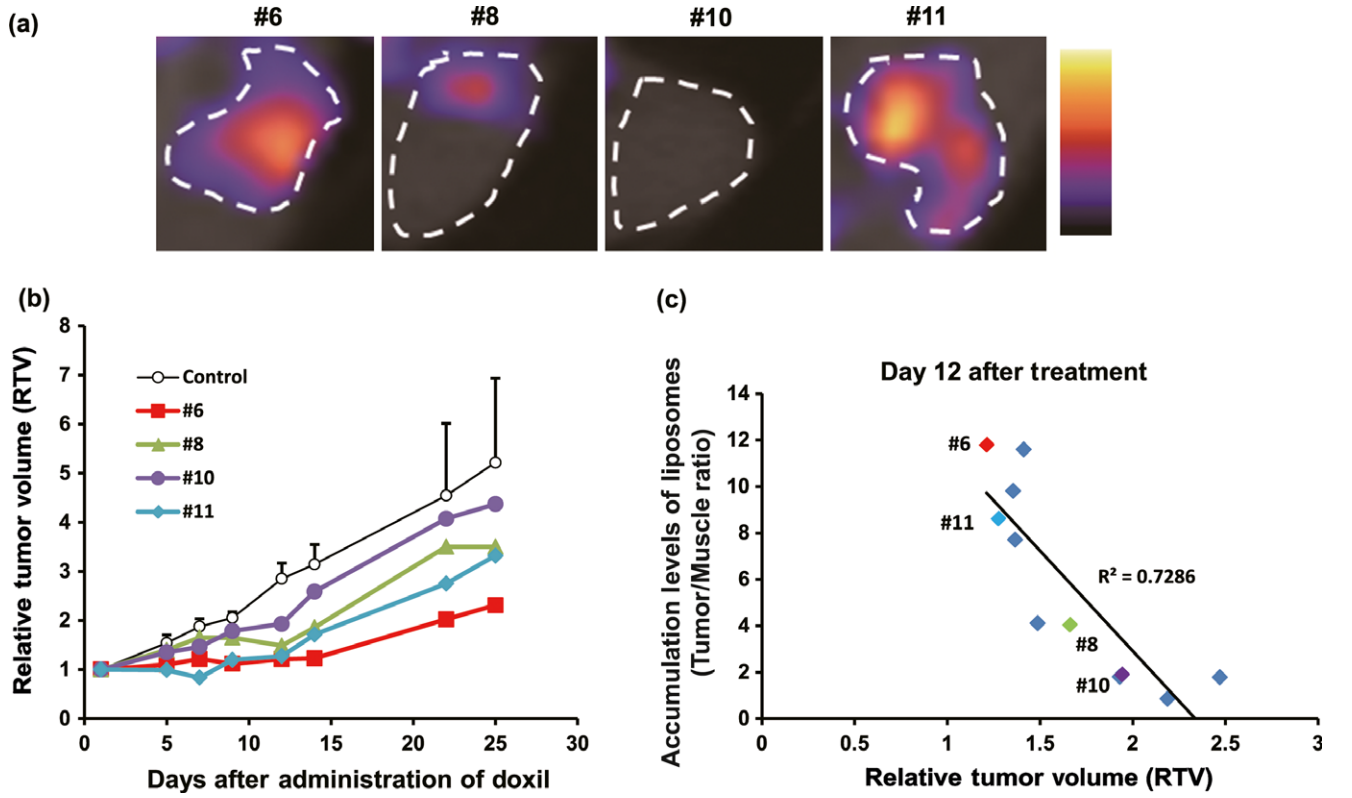

Fig. 5. Correlation analysis between accumulation of ^{111}In-encapsulated liposomes in tumor and antitumor activity of doxorubicin-encapsulated liposome (Doxil®). (a) Representative single-photon emission computed tomography (SPECT)/CT images of mice (#6, #8, #10, and #11) that were xenografted with SK-OV-3 tumor (n = 11). Images were obtained 72 h after injection of the radiolabeled liposomes. White circles indicate the tumor region based on superimposed CT images. (b) Graph showing representative relative antitumor effects of Doxil® (n = 11) versus control mice (n = 11). (c) Correlation analysis between accumulation of ^{111}In-encapsulated liposomes in SK-OV-3 xenografted tumors and antitumor activity of Doxil®.

change in response to treatment. Our approach will contribute considerably to optimize cancer therapy toward personalized medicine.

The SPECT/CT tests have already been introduced in actual clinical practice, and they are used to evaluate the biodistribution patterns of radiopharmaceuticals with quantitative indices. ^{111}In is one of the popular radionuclides in clinical nuclear medicine, and human studies with radiolabeled liposomes have already been carried out with no serious complications.[30] Therefore, our approach using ^{111}In-encapsulated liposomes to determine the indications for liposomal anticancer agents can feasibly be translated to the clinical setting. In conclusion, our integrated preclinical study clearly provides, for the first time, correlations between the therapeutic effects of Doxil® and histological factors associated with EPR. Furthermore, our results clearly indicate that tumor accumulation of the radiolabeled liposomes due to EPR effects could efficiently be evaluated by SPECT/CT tests. Our preclinical experimental validation shows the applicability of SPECT/CT imaging with radiolabeled liposomes to properly decide the indications for liposomal anticancer agents with significant potential towards clinical practice.

Acknowledgments

We wish to thank Dr. Hiroshi Ishihara, Dr. Kenji Hyodo, and Dr. Hiroshi Kikuchi for critical reading of the manuscript, and Ms. Yoko Yoshida, Dr. Takanori Abe, Dr. Tsuyoshi Akagi, Dr. Hiroshi Shirota, and Dr. Akira Yokoi for their support with *in vivo* experiments. This work was partially supported by a Grant-in-Aid for Young Scientists B (S.H., 26861034), a Grant-in-Aid for Scientific Research B (I.O.U., 24390297, 15H04911), a Grant-in-Aid for Challenging Exploratory Research (I.O.U., 25670546), and a Grant-in-Aid for Scientific Research on Innovative Areas (H.F., 23112525) from the Japan Society for the Promotion of Science. This work was also financially supported by Eisai, Co., Ltd. under the provisions of the collaborative contract between the National Cancer Center and Eisai, Co., Ltd.

Disclosure Statement

K.I., M.A., Y.H., J.M., M.I., and Y.F. are employees of Eisai Co., Ltd. H.F. is financially supported by Eisai, Co., Ltd. and Nihon-Mediphysics, Co., Ltd. under the provisions of the collaboration contract between the National Cancer Center and these companies.

References

1 Dawidczyk CM, Kim C, Park JH *et al.* State-of-the-art in design rules for drug delivery platforms: lessons learned from FDA-approved nanomedicines. *J Controlled Release* 2014; **10**: 133–44.
2 Chamberlain MC. Neurotoxicity of intra-CSF liposomal cytarabine (DepoCyt) administered for the treatment of leptomeningeal metastases: a retrospective case series. *J Neurooncol* 2012; **109**: 143–48.
3 Maeda H. Tumor-selective delivery of macromolecular drugs via the EPR effect: background and future prospects. *Bioconjug Chem* 2010; **21**: 797–802.

4 Maeda H, Matsumura Y. EPR effect based drug design and clinical outlook for enhanced cancer chemotherapy. *Adv Drug Deliv Rev* 2011; **63**: 129–30.
5 Maeda H, Nakamura H, Fang J. The EPR effect for macromolecular drug delivery to solid tumors: improvement of tumor uptake, lowering of systemic toxicity, and distinct tumor imaging in vivo. *Adv Drug Deliv Rev* 2013; **65**: 71–9.
6 Matsumura Y, Maeda H. A new concept for macromolecular therapeutics in cancer chemotherapy: mechanism of tumoritropic accumulation of proteins and the antitumor agent smancs. *Cancer Res* 1986; **46**: 6387–92.
7 Barenholz Y. Doxil(R) – the first FDA-approved nano-drug: lessons learned. *J Controlled Release* 2012; **160**: 117–34.
8 Safra T, Muggia F, Jeffers S *et al.* Pegylated liposomal doxorubicin (doxil): reduced clinical cardiotoxicity in patients reaching or exceeding cumulative doses of 500 mg/m^2. *Ann Oncol* 2000; **11**: 1029–33.
9 O'Brien ME, Wigler N, Inbar M *et al.* Reduced cardiotoxicity and comparable efficacy in a phase III trial of pegylated liposomal doxorubicin HCl (CAELYX/Doxil) versus conventional doxorubicin for first-line treatment of metastatic breast cancer. *Ann Oncol* 2004; **15**: 440–49.
10 Deitcher OR, Glaspy J, Gonzalez R *et al.* High-dose vincristine sulfate liposome injection (Marqibo) Is not associated with clinically meaningful hematologic toxicity. *Clin Lymphoma Myeloma Leuk* 2014; **14**: 197–202.
11 Gill PS, Wernz J, Scadden DT *et al.* Randomized phase III trial of liposomal daunorubicin versus doxorubicin, bleomycin, and vincristine in AIDS-related Kaposi's sarcoma. *J Clin Oncol* 1996; **14**: 2353–64.
12 Gordon AN, Fleagle JT, Guthrie D *et al.* Recurrent epithelial ovarian carcinoma: a randomized phase III study of pegylated liposomal doxorubicin versus topotecan. *J Clin Oncol* 2001; **19**: 3312–22.
13 Muggia FM, Hainsworth JD, Jeffers S *et al.* Phase II study of liposomal doxorubicin in refractory ovarian cancer: antitumor activity and toxicity modification by liposomal encapsulation. *J Clin Oncol* 1997; **15**: 987–93.
14 James ML, Gambhir SS. A molecular imaging primer: modalities, imaging agents, and applications. *Physiol Rev* 2012; **92**: 897–965.
15 Willmann JK, van Bruggen N, Dinkelborg LM *et al.* Molecular imaging in drug development. *Nat Rev Drug Discovery* 2008; **7**: 591–607.
16 Kwekkeboom DJ, Kam BL, van Essen M *et al.* Somatostatin receptor-based imaging and therapy of gastroenteropancreatic neuroendocrine tumors. *Endocr Relat Cancer* 2010; **17**: R53–73.
17 Li S, Goins B, Zhang L, Bao A. A novel multifunctional theranostic liposome drug delivery system: construction, characterization, and multimodality MR, near-infrared fluorescent and nuclear imaging. *Bioconjug Chem* 2012; **23**: 1322–32.
18 de Barros AB, Tsourkas A, Saboury B, Cardoso VN, Alavi A. Emerging role of radiolabeled nanoparticles as an effective diagnostic technique. *EJNMMI Res* 2012; **2**(1): 39.
19 Petersen AL, Hansen AE, Gabizon A *et al.* Liposome imaging agents in personalized medicine. *Adv Drug Deliv Rev* 2012; **64**: 1417–35.
20 Salmon HW, Siemann DW. Effect of the second-generation vascular disrupting agent OXi4503 on tumor vascularity. *Clin Cancer Res* 2006; **12**: 4090–94.
21 Ogihara-Umeda I, Sasaki T, Kojima S *et al.* Optimal radiolabeled liposomes for tumor imaging. *J Nucl Med* 1996; **37**: 326–32.
22 Umeda IO, Tani K, Tsuda K *et al.* High resolution SPECT imaging for visualization of intratumoral heterogeneity using a SPECT/CT scanner dedicated for small animal imaging. *Ann Nucl Med* 2012; **26**: 67–76.
23 Dams ET, Oyen WJ, Boerman OC *et al.* 99mTc-PEG liposomes for the scintigraphic detection of infection and inflammation: clinical evaluation. *J Nucl Med* 2000; **41**: 622–30.
24 Gabizon A, Chisin R, Amselem S *et al.* Pharmacokinetic and imaging studies in patients receiving a formulation of liposome-associated adriamycin. *Br J Cancer* 1991; **64**: 1125–32.
25 Dewaraja YK, Wilderman SJ, Koral KF *et al.* Use of integrated SPECT/CT imaging for tumor dosimetry in I-131 radioimmunotherapy: a pilot patient study. *Cancer Biother Radiopharm* 2009; **24**: 417–26.
26 Harrington KJ, Mohammadtaghi S, Uster PS *et al.* Effective targeting of solid tumors in patients with locally advanced cancers by radiolabeled pegylated liposomes. *Clin Cancer Res* 2001; **7**: 243–54.
27 Fang J, Nakamura H, Maeda H. The EPR effect: unique features of tumor blood vessels for drug delivery, factors involved, and limitations and augmentation of the effect. *Adv Drug Deliv Rev* 2011; **63**: 136–51.
28 Shcherbinin S, Chamoiseau S, Celler A. Quantitative image reconstruction for dual-isotope parathyroid SPECT/CT: phantom experiments and sample patient studies. *Phys Med Biol* 2012; **57**: 4755–69.
29 Grimes J, Celler A, Shcherbinin S *et al.* The accuracy and reproducibility of SPECT target volumes and activities estimated using an iterative adaptive thresholding technique. *Nucl Med Commun* 2012; **33**: 1254–66.
30 Kubo A, Nakamura K, Sammiya T *et al.* Indium-111-labelled liposomes: dosimetry and tumour detection in patients with cancer. *Eur J Nucl Med* 1993; **20**: 107–13.

Supporting Information

Additional supporting information may be found in the online version of this article:

Data S1. Supplementary materials and methods.

Fig. S1. Representative serial single-photon emission computed tomography (SPECT)/CT images of xenografted human ovarian cancers.

Fig. S2. Histopathological analyses between tumor perfusion levels and several parameters.

Table S1. *In vivo* antitumor effect of doxorubicin and enhanced efficacies of doxorubicin-encapsulated liposome (Doxil®).

Table S2. Stability of ^{111}In-encapsulated liposomes in mouse serum.

Table S3. Biodistribution of ^{111}In-encapsulated liposomes in ovarian cancer xenograft models.